

See discussions, stats, and author profiles for this publication at: <https://www.researchgate.net/publication/275256219>

# Tertiary Carbonate Side Chains: Easily Tunable Thermo-labile Breaking Points for Controlling the Solubility of Conjugated Polymers

ARTICLE *in* CHEMISTRY OF MATERIALS · APRIL 2015

Impact Factor: 8.35 · DOI: 10.1021/acs.chemmater.5b00549

---

CITATION

1

READS

30

## 8 AUTHORS, INCLUDING:



[Tomasz Marszalek](#)

Max Planck Institute for Polymer Research

29 PUBLICATIONS 184 CITATIONS

[SEE PROFILE](#)



[Wojciech Pisula](#)

Max Planck Institute for Polymer Research

213 PUBLICATIONS 9,023 CITATIONS

[SEE PROFILE](#)



[Alexander Colsmann](#)

Karlsruhe Institute of Technology

78 PUBLICATIONS 980 CITATIONS

[SEE PROFILE](#)



[Manuel Hamburger](#)

Merck Group

23 PUBLICATIONS 143 CITATIONS

[SEE PROFILE](#)

# Tertiary Carbonate Side Chains: Easily Tunable Thermo-labile Breaking Points for Controlling the Solubility of Conjugated Polymers

Marius Kuhn,<sup>†,||</sup> Jens Ludwig,<sup>‡</sup> Tomasz Marszalek,<sup>§</sup> Torben Adermann,<sup>†,||</sup> Wojciech Pisula,<sup>§</sup> Klaus Müllen,<sup>§,||</sup> Alexander Colsmann,<sup>‡</sup> and Manuel Hamburger<sup>\*,†,||</sup>

<sup>†</sup>Institute of Organic Chemistry, Heidelberg University, Im Neuenheimer Feld 270, 69120 Heidelberg, Germany

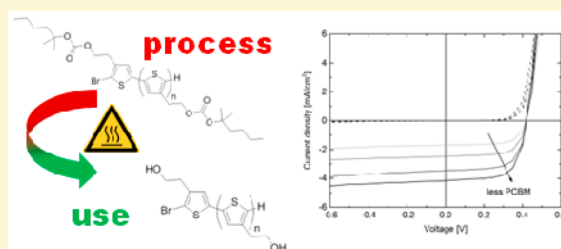
<sup>‡</sup>Light Technology Institute, Karlsruhe Institute of Technology (KIT), Engesserstrasse 13, 76131 Karlsruhe, Germany

<sup>§</sup>Max Planck Institute for Polymer Research, Ackermannweg 10, 55128 Mainz, Germany

<sup>||</sup>InnovationLab GmbH, Speyerer Strasse 4, 69115 Heidelberg, Germany

## S Supporting Information

**ABSTRACT:** We present a new class of solubilizing groups for conjugated polymers that enable solution processing of multilayer devices. Conjugated polymers in organic devices are sometimes difficult to process, because of their limited solubility. Well-soluble polymers decorated with alkyl side chains, however, introduce new challenges for thin-film deposition. Using the same solvent for multiple layers can dissolve the already applied layers. In this work, we introduce a new class of thermo-labile groups, which reduce the solubility of conjugated polymers after thermal treatment. Following a very modular approach, we can tune the temperature of the thermo-cleavage between 140 °C and 200 °C. This enables the fabrication of organic solar cells and field-effect transistors (FETs) with robust, solvent-resistant active layers.



## 1. INTRODUCTION

The unique optical, electrical, and film-forming properties of  $\pi$ -conjugated polymers enable various optoelectronic applications.<sup>1</sup> However, using soluble polymers opens new processing challenges for the fabrication of more-sophisticated device architectures. To make conjugated organic materials solution-processable, the introduction of solubilizing groups is often necessary,<sup>2</sup> although these groups can dramatically influence the solid-state structure of these compounds (e.g., their overall crystallinity or packing).<sup>3–6</sup> It is hardly possible to use the same or similar solvents for the deposition of consecutive layers, because of the dissolution of the layers that were already applied. Different approaches addressed this issue, which are based on cross-linking,<sup>7,8</sup> the use of orthogonal solvents,<sup>9,10</sup> or treatment with an external stimulus, such as heat,<sup>11–13</sup> all to prevent the dissolution of the previously formed layers. Especially, the treatment of the processed layers with heat, first reported by the Frechet group<sup>8</sup> and made technologically viable by the Krebs group,<sup>9</sup> using carboxylic acid ester pyrolysis/decarboxylation as thermo-cleavage for polythiophenes,<sup>14,15</sup> set the basis for our work. The disadvantage of this particular approach is the direct connection of the ester group to the polymer backbone, which causes changes in the electronic properties of the polymers, as observed for various substituted polythiophenes.<sup>16</sup> Another drawback is the high decarboxylation temperature (300 °C) that is necessary to yield

a semiconducting polythiophene that is compatible only with very heat-resistant flexible substrates.<sup>17</sup>

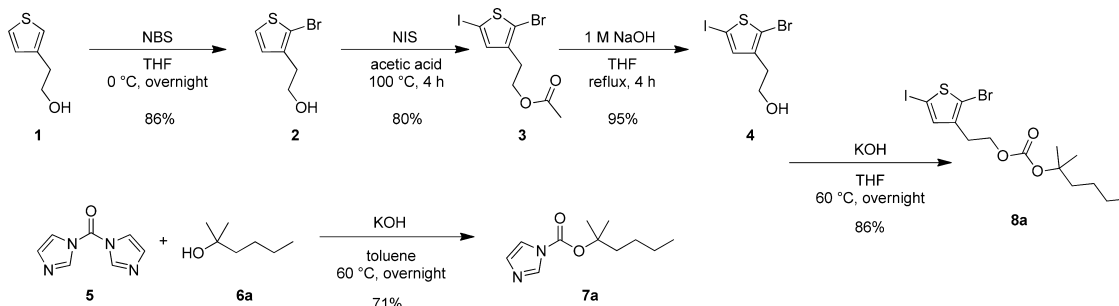
In this paper, we show that placing a spacer between the polymer backbone and the cleavable side chain helps to improve both issues. Although our spacer can universally attached to various conjugated polymers, we deliberately chose polythiophenes as the investigated model system to allow comparison to the literature. The electronic nature of the polythiophene remains unperturbed by the bond scissions before heat treatment, as well as after heat treatment. To reduce the cleavage temperature, we introduce a new thermo-labile group that is based on unsymmetrical carbonates with one tertiary alcohol. Leaving a hydroxyl function on the polymeric backbone after thermal removal, these carbonates and their cleavage temperature can be modified by changing the structure of the solubilizing side chain. This is very important for the goal of printing, drying, and pyrolyzing these polymers (poly(3-(2-((alkoxycarbonyl)oxy)ethyl)thiophen-2,5-diyls, P3COET) on low-cost flexible substrates such as polyethylene terephthalate (PET), since this limits the potential process temperatures to ~140 °C.

Received: February 11, 2015

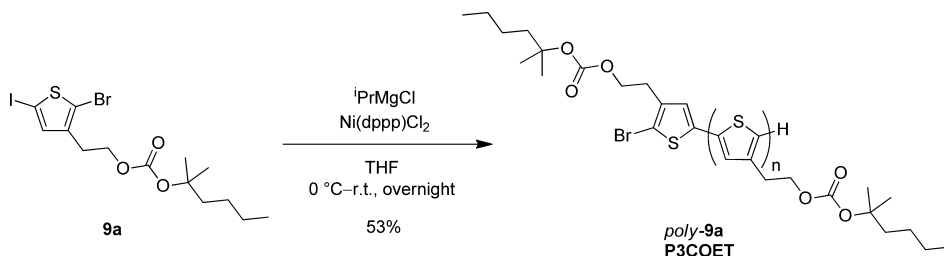
Revised: March 20, 2015

Published: March 23, 2015

**Scheme 1. Synthesis of Hydroxyl-Alkyl Functionalized Thiophene Monomer 4 and Its Modification with a Thermo-labile Solubilizing Carbonate Ester**



**Scheme 2. KCT Polymerization of the Thermo-labile Thiophene Monomer 9a To Give P3COET *poly*-9a**



## 2. RESULTS AND DISCUSSION

**2.1. Synthesis.** The synthetic route to the thermo-cleavable thiophene monomer is outlined in Scheme 1. The synthesis of the thiophene building block was carried out by a bromination of commercially available 2-(3-thienyl)ethanol (**1**) with *N*-bromosuccinimide (NBS), iodination with *N*-iodosuccinimide (NIS), and hydrolysis of the resulting ester **3** to yield 2-(2-bromo-5-iodothiophen-3-yl)ethanol (**4**). The ethandiy spacer of the 2-(2-bromo-5-iodothiophen-3-yl)ethanol (**4**) was chosen to exclude interference of the carbonate and the hydroxyl function after the cleavage, respectively, with the polymer backbone. It also allows varying the functional groups on the carbonate in a last step before polymerization.

The imidazole-*N*-carboxylic ester **7** was obtained by coupling 2-methylhexan-2-ol (**6a**) and 1,1'-carbonyldiimidazole (CDI, **5**), according to the synthetic procedure by Rannard.<sup>18</sup> The reason for using 2-methylhexan-2-ol (**6a**) as solubilizing alkyl chain was a compromise, given that the solubility between the uncleaved and cleaved polymer should be maximized while, on the other hand, producing volatile fragments.<sup>8,9</sup>

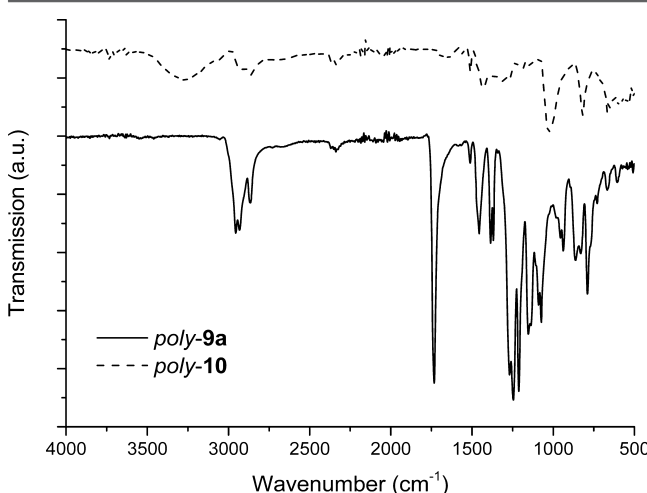
The synthesis of the final carbonate **9a** could be improved by switching the solvent from toluene (50% yield) to tetrahydrofuran (86% yield). The polymerization (**9a** to *Poly*-**9a**, Scheme 2) was performed using the Kumada catalyst transfer polymerization (KCTP) reported by Yokozawa.<sup>19</sup> The low reaction temperature is ideal for the polymerization of thermo-labile thiophenes **9**, so that no cleavage of the thermo-labile solubilizing chains can occur.

After precipitation from methanol and Soxhlet extraction, the new P3COET polymer *Poly*-**9a** was characterized by size exclusion chromatography, while the regioregularity was measured by <sup>1</sup>H NMR spectroscopy. The P3COETs were purified and fractionated by Soxhlet extraction with different solvents (methanol followed by acetone and chloroform). The methanol fraction contained only monomers and oligomers, and the acetone and chloroform fractions provided two polythiophenes:

- acetone fraction (39%):  $M_n = 15.3 \text{ kg/mol}$ ,  $M_w = 24.6 \text{ kg/mol}$ , PDI = 1.6; and
- chloroform fraction (15%):  $M_n = 41.0 \text{ kg/mol}$ ,  $M_w = 45.6 \text{ kg/mol}$ , PDI = 1.1.

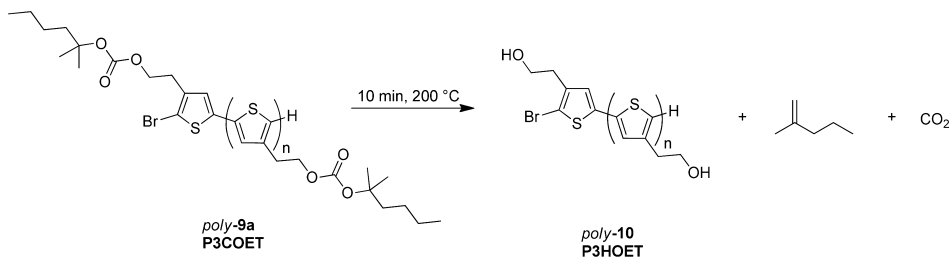
### 2.2. Characterization of *Poly*-**9a** and Its Pyrolysis Product.

**Product.** Infrared (IR) spectroscopy is a very convenient analytical characterization technique to indicate whether the polymer consists of carbonates only or already has some cleaved functionalities on the backbone (i.e., alcohols). Figure 1



**Figure 1.** IR spectra of P3COET *Poly*-**9a** (solid trace) and P3HOET *Poly*-**10** (dashed trace).

shows IR spectra before (dashed) and after (solid) the cleavage, which clearly show the split-off of the solubilizing group. The carbonates in *Poly*-**9a** give rise to a strong band at  $1737 \text{ cm}^{-1}$ , which can be assigned to the carbonyl stretching mode. After the cleavage, the carbonyl band disappears completely and the liberated alcohol functionality ( $3230 \text{ cm}^{-1}$ ) of P3HOET *Poly*-**10** (poly-3-(2-hydroxyethyl)thiophene-2,5-diyl) can be de-

**Scheme 3.** Decomposition Reaction of P3COET *poly-9a* to P3HOET *poly-10* after Heating at 200 °C for 10 min

tected. (Scheme 3 shows the decomposition of P3COET *poly-9a* to P3HOET *poly-10* after heating at 200 °C for 10 min.)

The relative (in)stability of the P3COETs was investigated by thermogravimetric analysis (TGA) in conjunction with differential scanning calorimetry (DSC) in the temperature range up to 300 °C (Figure 2). The carrier gas leaving the

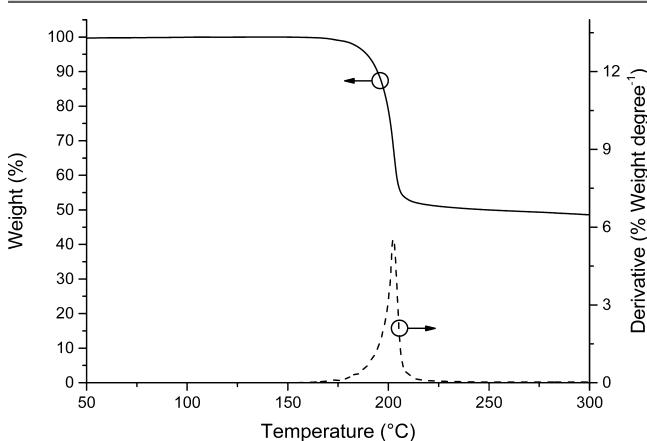


**Figure 2.** Thermogravimetric analysis of P3COET *poly-9a* in the temperature range of 50–300 °C. The data was recorded at an increasing temperature of 10 °C min<sup>-1</sup> under nitrogen atmosphere. A derivative weight loss curve has been included to indicate the point with the most apparent weight loss.

furnace was analyzed by mass spectrometry and Fourier transform infrared spectroscopy (TGA-MS-FTIR, see the Supporting Information). These measurements corroborate the evaporation of 2-methyl-2-hexene and carbon dioxide from the sample starting at 180 °C, reaching its maximum at 200 °C.

The optical and electronic properties of the carbonate-functionalized polythiophene *poly-9a* were investigated by ultraviolet-visible (UV-vis) spectroscopy and cyclic voltammetry (CV) measurements (see the Supporting Information). The introduction of the carbonate with a C<sub>2</sub>-spacer has a small effect on the UV-vis spectra of the polythiophene. This hints to a slightly higher nonplanarity of the conjugated backbone than in common poly(3-hexylthiophene) (P3HT), because of the different length and steric demand of the solubilizing alkyl chain.<sup>3</sup> The CV measurement (*poly-9a* film in acetonitrile against Fc/Fc<sup>+</sup>) confirms the equal electronic properties of the polythiophene *poly-9a* (*E*<sub>ox</sub> = 0.52 V), compared to P3HT.<sup>20</sup>

**2.3. Control of Cleavage Temperature.** To enable the use of our thermo-labile polymers on low-cost flexible substrates (such as PET, for example), their structure should be modified to reduce the cleavage temperature to ~140 °C. *Ab initio* and experimental studies by Van Speybroeck revealed that a six-membered cyclic transition state is required to have an optimal geometry, while the C<sub>α</sub>–O bond dissociation is the

rate-determining step. Stabilization of the positive charge in the C<sub>α</sub> position affects acceleration of the reaction rate. The last step is a β-H-elimination or *syn*-elimination.<sup>21,22</sup>

According to this mechanism, it is possible to tune the elimination temperature by changing the cation-stabilizing properties of the side chain. Based on this rationale, we set out to prepare derivatives changing the alkyl into an alkenyl (**6h**–**6j**) or alkynyl (**6e**–**6g**) side chains, which form mesomerically stabilized cations and eventually lead to conjugated double bonds after elimination. The two methyl groups or a cyclic group next to the alcohol are necessary for stabilization and simultaneously provide β-H for the pyrolysis. The corresponding alcohols were synthesized by nucleophilic addition of Grignard reagents to carboxyl functions or lithiated alkynes to acetone, cyclopentanone or cyclohexanone, respectively. All synthesized alcohols were stable, and most of them could be obtained in good to excellent yields (see Table 1 and the Supporting Information).

The synthesis of the imidazole-N-carboxylic esters **7** proved necessary for the synthesis of the asymmetric carbonates and

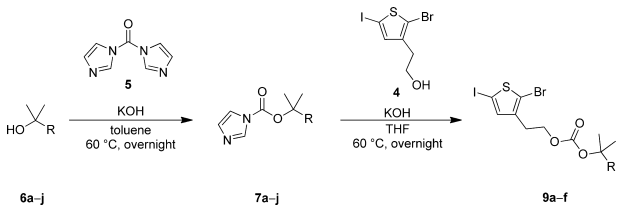
**Table 1.** Chemical Structures and Yields of the Alcohols, Carboxyl Esters, and Carbonates Prepared in This Study

| Solubilizing group | Alcohol, yield             | Imidazole-N-carboxylic ester, yield | Carbonate, yield             |
|--------------------|----------------------------|-------------------------------------|------------------------------|
|                    | <b>6a</b> , – <sup>a</sup> | <b>7a</b> , 86%                     | <b>9a</b> , 86%              |
|                    | <b>6b</b> , – <sup>a</sup> | <b>7b</b> , 70%                     | <b>9b</b> , 84%              |
|                    | <b>6c</b> , 70%            | <b>7c</b> , 31%                     | <b>9c</b> , 91%              |
|                    | <b>6d</b> , 45%            | <b>7d</b> , 46%                     | <b>9d</b> , 74%              |
|                    | <b>6e</b> , 78%            | <b>7e</b> , 74%                     | <b>9e</b> , 90% <sup>c</sup> |
|                    | <b>6f</b> , 91%            | <b>7f</b> , 85%                     | <b>9f</b> , 80% <sup>c</sup> |
|                    | <b>6g</b> , 78%            | <b>7g</b> , 17%                     | –                            |
|                    | <b>6h</b> , 63%            | –, <b>8h</b> <sup>b</sup>           | –                            |
|                    | <b>6i</b> , 94%            | –, <b>8i</b> <sup>b</sup>           | –                            |
|                    | <b>6j</b> , quant.         | –, <b>8j</b> <sup>b</sup>           | –                            |

<sup>a</sup>Commercially available. <sup>b</sup>No imidazole-N-carboxylic esters were isolated, but the decarboxylated N-substituted imidazoles **8h** and **8i** were formed. <sup>c</sup>triethylamine added for purification by column chromatography.

were obtained by coupling the appropriate alcohol **6** and 1,1'-carbonyldiimidazole (CDI, **5**). Interestingly, during these reactions or their workup, some imidazole-*N*-carboxylic esters already decomposed. The CDI-coupling of allylic or benzylic alcohols did not yield the imidazole-*N*-carboxylic esters but the decarboxylated *N*-substituted imidazoles (**8h–8j**, see the Supporting Information) were formed. This was a first hint that some imidazole-*N*-carboxylic esters and the corresponding carbonates were not stable enough to synthesize a polymer. The carbonate monomers **9** finally were obtained by reacting the imidazole-*N*-carboxylic esters **7** with 2-(2-bromo-5-iodothiophen-3-yl)ethanol (**4**). (See Scheme 4.) For some of

**Scheme 4. Syntheses of the 3-(2-((alkoxycarbonyl)oxy)ethyl)thiophene Monomers **9**, Starting from Tertiary Alcohols **6****



the monomers (**9e** and **9f**), triethylamine had to be added to the eluent during purification by column chromatography, since the silica gel was otherwise too acidic for the carbonate groups. The use of acidic additives to lower the cleaving temperature has already been shown by the Krebs group.<sup>23</sup> The yields of the respective imidazole-*N*-carboxylic ester syntheses allow a good forecast for the stability of the resulting carbonates **9**. We observed that imidazole-*N*-carboxylic ester **7g** with a cyclopentyl and alkynyl side chain (entry 7) was difficult to isolate and that the carbonate **9g** could not be obtained. The cyclopentyl group resulted in less stable compounds than the cyclohexyl.

With this set of monomers, the corresponding polymers (Table 2) were prepared by KCT polymerization.<sup>16</sup> (See Scheme 5.) The low reaction temperature of this reaction proves ideal for the polymerization of the monomers **9**, since it prohibits the cleavage of the thermo-labile solubilizing chains during polymerization.

Table 2 is a compilation of all synthesized P3COETs **poly-9a–9f**. Obviously, the yields correlate with the cleavage temperature of the thermo-labile solubilizing chains and results from the purification method. P3COETs with lower cleavage temperatures, such as **poly-9c–9f** (Table 2), partially cleave during the synthesis or the purification by Soxhlet extraction, because of the high temperature and the slight acidic behavior of chloroform.<sup>20</sup> In this case, formation of insoluble P3HOET **poly-10** in the Soxhlet thimble could be observed, but also the soluble polymers **poly-9c** and **poly-9d** already exhibit a small hydroxyl band in their IR spectra. The other P3COETs show no hydroxyl vibrations in the IR analysis, which is consistent with a higher cleavage temperature. The molecular weights ( $M_w$ ) of the polymers are in the range of 4.8–45.6 kg mol<sup>-1</sup> and are not linked to the yields or the (in)stability (entry 3 in Table 2). The dispersity (PDI) of the polymers is low. Figure 3 shows the thermal behavior of the P3COETs **poly-9a–9f** as normalized TGA curves in the temperature range of 100–250 °C. The range of the thermal cleavage is between 140 °C (**poly-9c**, entry 3 in Table 2) and 198 °C (**poly-9b**, entry 2 in Table

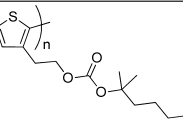
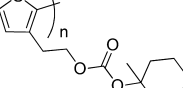
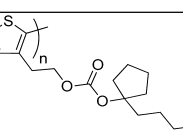
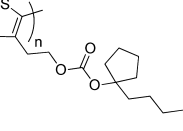
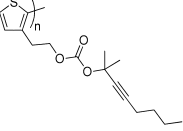
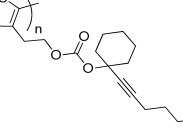
2). The polymers with cyclopentyl groups (**poly-9c** and **poly-9d**; entries 3 and 4 in Table 2) are less stable than the polymers with alkynyl groups (**poly-9e** and **poly-9f**; entries 5 and 6 in Table 2). The **poly-9b** with a cyclohexyl group (entry 2 in Table 2) exhibits the highest cleavage temperature. The difference in the normalized TGA curve shapes is dependent on the boiling point of the alkene generated during the pyrolysis.

**2.4. Thin Film Structural Analysis.** The control over the surface arrangement of conjugated polymers is essential for their application in electronic devices. Generally, transistors require an edge-on polymer arrangement favoring the charge carrier transport parallel to the dielectric surface.<sup>24</sup> On the other hand, the efficiency of solar cells can be improved by a face-on assembly when the  $\pi$ -stacking direction is oriented perpendicular to the substrate and, thus, in the direction of the charge carrier transport. Different approaches related to polymer design and processing have been reported to control the surface organization of polymers. For instance, the morphology of P3HT thin films can be tuned by substrate treatment<sup>25</sup> and the solvents used for thin-film fabrication.<sup>26</sup> The annealing of a polymer at its melting temperature can also change the surface organization as in the case of polynaphthalene–bithiophene from face-on, obtained after spin-coating, to edge-on.<sup>27</sup> Concerning the polymer design, the organization of P3HT can be controlled by its regioregularity.<sup>28</sup> The aggregation in solution also plays an important role and is affected by the polymer interactions. Polymers with bulky substituents reducing aggregation assemble on the surface face-on, while macromolecules with strong interactions and subsequent aggregation in solution are arranged edge-on.<sup>29</sup> In bulk-heterojunction structures for solar cells, PCBM acts as a plasticizer for the conjugated polymers and can induce reorganization of the polymer mostly to a face-on construction, thus enhancing the device efficiency.<sup>30</sup>

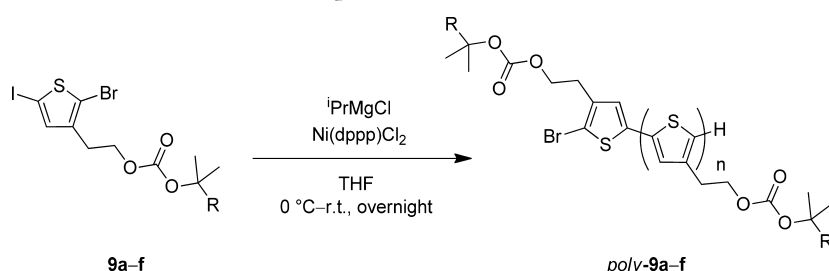
**2.4.1. Neat P3COET Polymer Films.** In order to identify differences in polymer organization before and after thermal cleavage of solution deposited thin films of P3COET **poly-9a**, grazing-incidence wide-angle X-ray scattering (GIWAXS) measurements were performed. Since **poly-9a** can be applied in at least two different types of devices (field-effect transistors and organic solar cells), two types of samples were investigated: pure P3COET and its blend with an acceptor. In the first case, drop-cast or spin-coated neat **poly-9a** samples were fabricated according to the procedures used for the transistor fabrication (see the Supporting Information).

Large variation in packing for **poly-9a** drop-cast films before and after annealing at 200 °C is evident from the GIWAXS patterns presented in Figure 4. Both patterns reveal quite isotropic reflections, indicating a rather random distribution of the crystallites toward the surface. This is not surprising, since the drop-cast films are relatively thick with no preferential growth direction of the polymers. Nevertheless, the maximum intensity of the *h*00 reflection on the meridional plane implies certain preference of the polymer orientation on the surface. This reflection is assigned to an interlayer distance of 2.20 nm of layers arranged parallel to the substrate with quasi edge-on polymer backbones. In comparison to regioregular P3HT ( $d = 1.57$  nm),<sup>31</sup> the larger layer spacing obtained for **poly-9a** is caused by the attached thermally sensitive alkyl chains. In addition, the substituents influence the interaction between polymers. The lack of a corresponding  $\pi$ -stacking peak of **poly-9a** before annealing suggests highly disordered polymer packing within the layer structures (Figure 4a).

Table 2. Chemical Structures, Yields, and Properties of P3COETs *poly-9a–9f* Obtained by KCT Polymerization of *9a–9f*

|                | Product   | Yield<br>[%] <sup>a</sup>          | M <sub>n</sub><br>[kg mol <sup>-1</sup> ] <sup>e</sup> | M <sub>w</sub><br>[kg mol <sup>-1</sup> ] <sup>e</sup> | PDI          | Cleavage<br>temperature <sup>f</sup><br>[°C] |
|----------------|---|------------------------------------|--|--|--------------|--|
| <i>poly-9a</i> |    | 39 <sup>b</sup><br>15 <sup>c</sup> | 15.3<br>41.0   | 24.6<br>45.6   | 1.61<br>1.11 | 192  |
| <i>poly-9b</i> |    | 25 <sup>c</sup>                    | 18.4   | 22.9   | 1.25         | 198  |
| <i>poly-9c</i> |    | 5 <sup>c</sup>                     | 22.0   | 27.5   | 1.24         | 140  |
| <i>poly-9d</i> |    | 3 <sup>b</sup><br>— <sup>d</sup>   | 4.3  | 4.8  | 1.11         | 168  |
| <i>poly-9e</i> |   | 20 <sup>c</sup>                    | 8.2  | 10.9   | 1.32         | 174  |
| <i>poly-9f</i> |  | 23 <sup>b</sup><br>— <sup>d</sup>  | 17.9   | 31.7   | 1.77         | 178  |

<sup>a</sup>After Soxhlet extraction. <sup>b</sup>Acetone-soluble. <sup>c</sup>Chloroform-soluble. <sup>d</sup>Nonsoluble fraction in chloroform obtained after cleavage. <sup>e</sup>Determined by SEC with polystyrene standards in chloroform. <sup>f</sup>Temperature at 5% weight loss, measured by thermogravimetric analysis (at 10 °C min<sup>-1</sup>).

Scheme 5. KCT Polymerization of Thermo-labile Thiophene Monomers *9a–9f* To Obtain a Series of P3COETs (cf. Table 2)

The GIWAXS pattern in Figure 4b is obtained for *poly-9a* after thermal cleavage of the substituents (i.e., P3HOET *poly-10*). The interlayer distance observed for the unannealed film is slightly reduced from 2.20 nm to 2.15 nm. In addition, a new reflection on the meridional plane is observed for  $q_z = 0.67 \text{ \AA}^{-1}$  and  $q_{xy} = 0 \text{ \AA}^{-1}$  related to a *d*-spacing of 0.93 nm. This value is in agreement with the diameter of the polymer after thermal cleavage. The appearance of this reflection indicates the coexistence of two structures with independent interlayer spacings of 2.15 and 0.93 nm. Most probably, the thick drop-cast film undergoes only part of the cleavage reaction, leading to the formation of both phases. The film heterogeneity is also

the reason for the low level of the charge carrier mobility in field-effect transistors of  $10^{-5} \text{ cm}^2/(\text{V s})$  before and after thermo-cleavage (see the Supporting Information). To ensure more-homogeneous thermo-cleavage in the thin spin-coated samples, the films were treated at lower temperatures for significantly longer annealing times. This process allows thermo-cleavage through the entire film, leading solely to an interlayer distance of 0.93 nm (see Figure S2 in the Supporting Information). Generally, the crystallinity of the spin-coated films is lower, in comparison to drop-casting, because of the longer evaporation time of the solvent and therefore extended kinetics of the structure growth in the latter case. A further

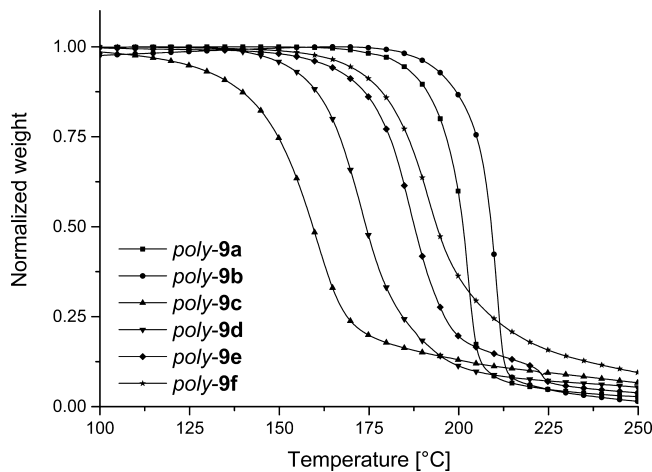


**Figure 3.** Normalized TGA curves of the P3COETs *poly-9a*–*9f*. The data was recorded at an increasing temperature rate of  $10\text{ }^{\circ}\text{C min}^{-1}$  under nitrogen atmosphere.

interesting change in the drop-cast film after the cleavage of the substituents is the increased packing order of the polymers, as is evident from the additional  $\pi$ -stacking reflection in the wide-angle scattering range related to a distance of 0.37 nm. It can be assumed that the steric demand of the substituent is reduced after thermo-cleavage, allowing a stronger interaction between the conjugated P3HOET backbones.

**2.4.2. Polymer:PCBM Films.** In order to integrate *poly-9a* into the absorber layers of bulk-heterojunction organic photovoltaic devices, we studied the thin-film formation of a polymer:fullerene blend upon deposition from solution. Therefore, we dissolved *poly-9a* and [6,6]-phenyl C<sub>61</sub>-butyric acid methyl ester (PCBM) 1:0.5 (wt:wt) in 1,2-dichlorobenzene and spin-cast the layer from the respective solution. We assessed the bulk-heterojunction homogeneity via atomic force microscopy (AFM). The thin-film topography of films that were annealed at 150 °C is depicted in Figure 5. The layers exhibited a root-mean-square roughness ( $r_q$ ) of ~0.36 nm and did not exhibit any pinholes. Upon annealing at 200 °C and hence above the cleavage temperature, the surface texture became rougher ( $r_q \approx 4.49$  nm) and, besides some larger aggregates, exhibited grains with a typical size of 10 nm that were randomly distributed all over the layer surface. Most

importantly, upon annealing, these layers were almost insoluble in the process solvent (i.e. 1,2-dichlorobenzene).

When investigated using X-ray diffraction (XRD), the effect of the thermo-cleavage on the polymer packing in *poly-9a* thin films is even more evident in the bulk-heterojunction structure. Figure 6 depicts the GIWAXS patterns obtained for thin spin-coated *poly-9a*:PCBM layers on *poly*(3,4-ethylenedioxythiophene):polystyrenesulfonate (PEDOT:PSS) before and after thermo-cleavage at 200 °C. The film before annealing is quite disordered, as only one single peak on the meridional plane at  $q_z = 0.285\text{ \AA}^{-1}$  and  $q_{xy} = 0\text{ \AA}^{-1}$  is observed. This reflection is assigned to the *poly-9a* interlayer distance of 2.20 nm, which is in agreement with the measurement of the drop-cast sample. Identical to the drop-cast film before thermal cleavage, no  $\pi$ -stacking reflection can be discerned for the spin-coated *poly-9a*:PCBM blend before annealing at 200 °C. As reported in the literature, PCBM does not show any crystalline organization up to an annealing temperature of 142 °C.<sup>32</sup> Annealing above the pyrolysis temperature (200 °C) drastically changes the GIWAXS pattern for the bulk-heterojunction structure. The main difference in the obtained pattern is the lack of the small-angle meridional reflection previously assigned to the layer arrangement. Interestingly, in the small-angle equatorial plane, new reflections at  $q_{xy} = 0.63\text{ \AA}^{-1}$  and  $q_z = 0\text{ \AA}^{-1}$  appear, corresponding to a *d*-spacing of 0.99 nm. This value is in agreement with the changes observed in the drop-cast and the spin-coated *poly-9a* film after thermal cleavage (see Figure S2 in the Supporting Information). However, in the bulk-heterojunction blend, the interlayer reflection moves from the meridional to equatorial plane, suggesting a change of the backbone organization from edge-on to face-on. Furthermore, the face-on organization after thermo-cleavage is confirmed by the appearance of the  $\pi$ -stacking reflection (0.38 nm) in the wide-angle meridional plane.

In this work, the rearrangement of *poly-9a* occurs after annealing and thermal cleavage of the substituents. The reorganization is attributed to the film plasticization by PCBM, increasing the mobility of the polymer chains during thermal cleavage.<sup>27</sup> During this annealing step, PCBM crystallizes as evident from the spotlike reflections observed in the off-meridional range of the pattern (Figure 6b) which has also been observed in the AFM measurements.<sup>29</sup> Consequently, the intralayer order increases, while the interlayer distance decreases. The higher order within the layers enhances the charge carrier transport in  $\pi$ -stacking direction, which, after the

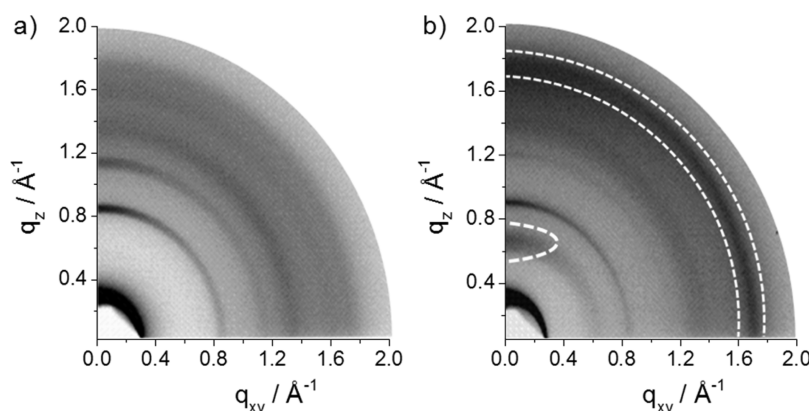


**Figure 4.** GIWAXS patterns of drop-cast films of *poly-9a* after annealing (a) at 100 °C and (b) at 200 °C. Meridional reflection related to the new interlayer and  $\pi$ -stacking peak are indicated by dashed circles.

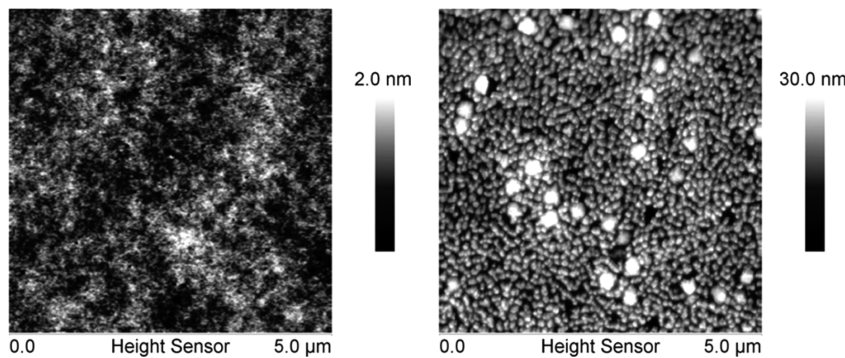


**Figure 5.** Surface texture of *poly-9a*:PCBM (1:0.5 wt/wt) films (a) after annealing at 150 °C and (b) after annealing at 200 °C and with side-chain cleavage.

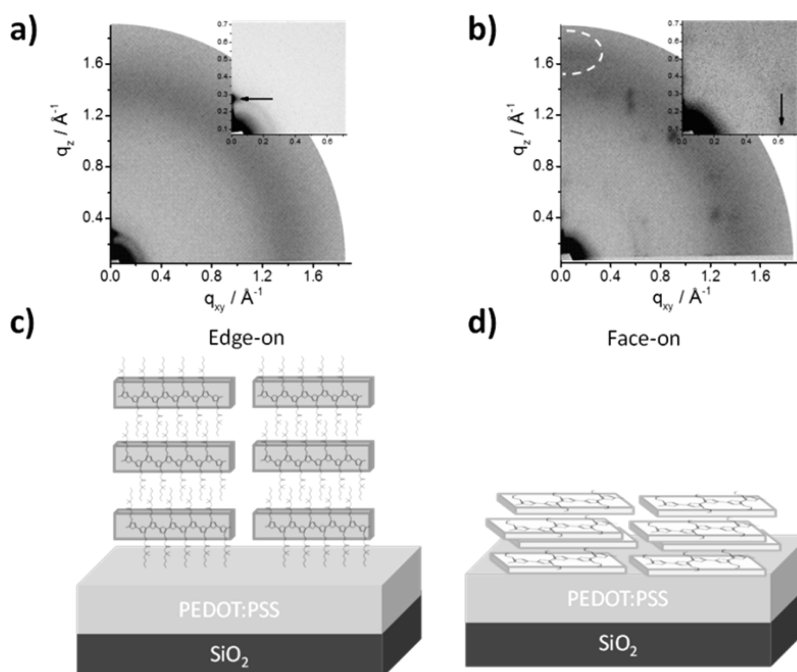


**Figure 6.** GIWAXS patterns of *poly-9a*:PCBM thin films on PEDOT:PSS (a) before and (b) after thermo-cleavage at 200 °C (meridional  $\pi$ -stacking reflection is indicated by the dashed circle). Insets show the small-range scattering range with the interlayer reflection indicated by an arrow. Schematic illustrations of the *poly-9a* surface organization obtained after fabrication with (c) edge-on and (d) face-on arrangement after thermal annealing at 200 °C (PCBM is omitted for the sake of simplicity).

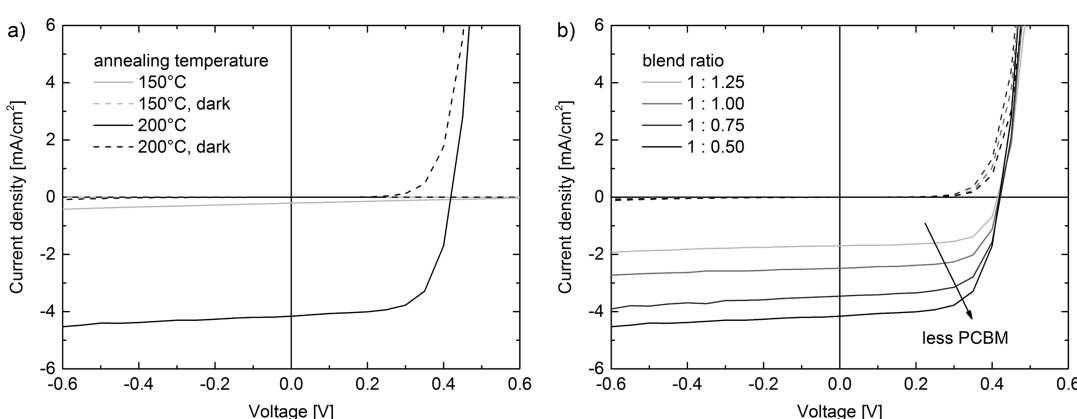


**Figure 7.** (a) Typical  $J$ – $V$  curves of *poly-9a*:PCBM (1:0.5 wt/wt) solar cells comprising photoactive layers that were annealed below the cleavage temperature (gray) and above the cleavage temperature (black), i.e., at 150 and 200 °C, respectively. (b) PCBM concentration-dependent  $J$ – $V$  measurements of devices that were annealed at 200 °C; the lower the PCBM load, the better the device performance (dashed lines represent dark curve measurement without illumination).

reorganization, coincides with the direction of the applied electric field in solar cells. In addition, the shorter interlayer periodicity and less-dense isolating alkyl mantle facilitates transport between layers. This increases the dimensionality of the charge carrier transport, allowing an easier bypassing of structural defects such as trapping sites.

**2.5. Bulk-Heterojunction Solar Cells.** The good film quality enabled the *poly-9a*:PCBM (1:0.5 wt/wt) layer integration into organic photovoltaic devices with an ITO/PEDOT:PSS/*poly-9a*:PCBM/Ca/Al device architecture. The solar cell with the absorber layer that was annealed at 150 °C, i.e., below the cleavage temperature, exhibits very poor performance, particularly because of a very low photo current, as depicted in Figure 7a. Upon annealing at 200 °C and side-chain cleavage, the photocurrent increases significantly to 4.2 mA/cm<sup>2</sup> and, hence, the device power conversion efficiency improves to 1.2% (see Table 3). This observation may be

**Table 3. Solar Cell Parameters for the Nontreated Solar Cell and the Thermally Treated Cells with Varying Polymer:Fullerene Ratio**

| polymer:fullerene blend ratio | annealing temperature [°C] | $J_{SC}$ [mA/cm <sup>2</sup> ] | $V_{OC}$ [V] | FF [%] | $\mu_{eff}$ [%] |
|-------------------------------|----------------------------|--------------------------------|--------------|--------|-----------------|
| 1:1.25                        | 200                        | 1.7                            | 0.41         | 68     | 0.5             |
| 1:1.0                         | 200                        | 2.5                            | 0.42         | 68     | 0.7             |
| 1:0.75                        | 200                        | 3.4                            | 0.42         | 69     | 1.0             |
| 1:0.5                         | 200                        | 4.2                            | 0.42         | 66     | 1.2             |
| 1:0.5                         | 150                        | 0.2                            | 0.68         | 24     | 0.03            |

attributed, in part, to the low PCBM load in the bulk heterojunction, which commonly depends on the degree of intercalation of polymer and fullerene. For optimized P3HT:PCBM solar cells, the blend ratio is on the order of 1:1. Here, the improvement of the device performance upon annealing at 200 °C and the removal of the side chains leads to a reduced intercalation. The reduced intercalation, in turn, enables better device efficiencies with reduced PCBM load. This assumption is supported by the concentration-dependent  $J$ – $V$  measurements that are depicted in Figure 7b, where we varied the *poly-9a*:PCBM blend ratio from 1:1.25 to 1:0.5. We clearly observe an enhancement of the photocurrent toward lower PCBM concentrations. Hence, the removal of the bulky side chains not only provides a change in layer solubility but also reduces the required amount of fullerenes in the bulk heterojunction.

### 3. CONCLUSION

We synthesized a series of novel carbonate-functionalized thiophene monomers and regioregular polythiophenes P3COETs of variable pyrolysis temperature. By tuning the stabilization of the cleavage fragments, we control the onset of the pyrolysis down to a temperature region that is compatible with low-cost polymeric substrates, such as PET. TGA measurements, in combination with infrared (IR) spectroscopic studies, verify the completeness and the selectivity of the cleavage to the corresponding P3HOET.

Based on untreated P3COETs, lateral charge transport was observed in TFTs. After the pyrolysis, however, no working TFT could be obtained. On the other hand, the efficiency of the solar cells was dramatically improved upon pyrolysis. This intriguing observation could be rationalized based on GIWAXS measurements in thin films of either pure P3COET, the

pyrolyzed P3HOET and the respective blends with PCBM on device-relevant substrates. These polythiophenes exhibit different preferential orientation, with respect to the surface from edge-on before cleavage and face-on after cleavage, which explains the observed swap in device performance.

Because of the mass loss during cleavage, the relative amount of PCBM necessary to obtain solar cells with maximum efficiency is drastically reduced, compared to noncleavable polythiophenes, such as P3HT.

The compounds presented in this study show the potential of thermo-cleavable solubilizing side chains with controllable cleavage temperature. The moderate process temperature enables device fabrication on low-cost substrates. The reduced diffusivity of the polymers after cleavage enables the generation of morphologically more-robust thin films, which may lead to long-term stability of the morphology. Cleaving off the side chains and hence significantly reducing the material solubility makes this concept interesting for future multilayer organic optoelectronic devices, in particular when transferred to high-performance amorphous polymers.

### ■ ASSOCIATED CONTENT

#### Supporting Information

Experimental and analytical data on all prepared compounds, thin film transistor and solar cell fabrication details, and characterization data is provided as Supporting Information. This material is available free of charge via the Internet at <http://pubs.acs.org>.

### ■ AUTHOR INFORMATION

#### Corresponding Author

\*E-mail: M.Hamburger@oci.uni-heidelberg.de.

#### Notes

The authors declare no competing financial interest.

### ■ ACKNOWLEDGMENTS

The authors like to thank U.H.F. Bunz for measuring time on his analytical equipment, as well as insightful discussions, and T. Gessner and T. Weitz (BASF SE) for TGA-MS-FTIR measurements. The Federal Ministry for Education and Research (BMBF) is acknowledged for funding under Contract No. 13N11701 (Project MORPHEUS). K.M. and T.M. acknowledge the ERC Advanced Grant NANOGRAPH (No. AdG-2010-267160). We also gratefully acknowledge the DELTA Electron Storage Ring (Dortmund, Germany) for providing synchrotron radiation and technical support in the GIWAXS measurements.

### ■ REFERENCES

- Pron, A.; Gawrys, P.; Zagorska, M.; Djuradoa, D.; Demadrillea, R. *Chem. Soc. Rev.* **2010**, *39*, 2577–2632.
- Mei, J.; Bao, Z. *Chem. Mater.* **2014**, *26*, 604–615.
- Hotta, S.; Rughooputh, S. D. D. V.; Heeger, A. J.; Wudl, F. *Macromolecules* **1987**, *20*, 212–215.
- Mei, J.; Kim do, H.; Ayzner, A. L.; Toney, M. F.; Bao, Z. *J. Am. Chem. Soc.* **2011**, *133*, 20130–20133.
- Lei, T.; Dou, J.-H.; Pei, J. *Adv. Mater.* **2012**, *24*, 6457–6461.
- Lei, T.; Wang, J.-Y.; Pei, J. *Chem. Mater.* **2014**, *26*, 594–603.
- Li, W.; Wang, Q.; Ji Cui, H. C.; Shaheen, S. E.; Jabbour, G. E.; Anderson, J.; Lee, P.; Kippelen, B.; Peyghambarian, N.; Armstrong, N. R.; Marks, T. J. *Adv. Mater.* **1999**, *11*, 730–734.
- Bayerl, M. S.; Braig, T.; Nuyken, O.; Müller, D. C.; Groß, M.; Meerholz, K. *Macromol. Rapid Commun.* **1999**, *20*, 224–228.
- Huang, F.; Wu, H.; Cao, Y. *Chem. Soc. Rev.* **2010**, *39*, 2500–2521.

- (10) Sax, S.; Rugen-Penkalla, N.; Neuhold, A.; Schuh, S.; Zojer, E.; List, E. J. W.; Müllen, K. *Adv. Mater.* **2010**, *22*, 2087–2091.
- (11) Liu, J.; Kadnikova, E. N.; Liu, Y.; McGehee, M. D.; Fréchet, J. M. J. *J. Am. Chem. Soc.* **2004**, *126*, 9486–9487.
- (12) Bjerring, M.; Nielsen, J. S.; Nielsen, N. C.; Krebs, F. C. *Macromolecules* **2007**, *40*, 6012–6013.
- (13) Yu, J.; Holdcroft, S. *Macromolecules* **2000**, *33*, 5073–5079.
- (14) Petersen, M. H.; Gevorgyan, S. A.; Krebs, F. C. *Macromolecules* **2008**, *41*, 8986–8994.
- (15) Hagemann, O.; Bjerring, M.; Nielsen, N. C.; Krebs, F. C. *Sol. Energy Mater. Sol. Cells* **2008**, *92*, 1327–1335.
- (16) Krebs, F. C.; Spanggaard, H. *Chem. Mater.* **2005**, *17*, 5235–5237.
- (17) Krebs, F. C.; Norrman, K. *ACS Appl. Mater. Interfaces* **2010**, *2*, 877–887.
- (18) Rannard, S. P.; Davis, N. J. *Org. Lett.* **1999**, *1*, 933–936.
- (19) Miyakoshi, R.; Yokoyama, A.; Yokozawa, T. *J. Am. Chem. Soc.* **2005**, *127*, 17542–17547.
- (20) Xin, H.; Guo, X.; Kim, F. S.; Ren, G.; Watson, M. D.; Jenekhe, S. A. *J. Mater. Chem.* **2009**, *19*, 5303–5310.
- (21) Speybroeck, V. V.; Martelé, Y.; Waroquier, M.; Schacht, E. J. *Am. Chem. Soc.* **2001**, *123*, 10650–10657.
- (22) Speybroeck, V. V.; Martelé, Y.; Schacht, E.; Waroquier, M. *J. Phys. Chem. A* **2002**, *106*, 12370–12375.
- (23) Søndergaard, R. R.; Norrman, K.; Krebs, F. C. *J. Polym. Sci., Part A: Polym. Chem.* **2012**, *50*, 1127–1132.
- (24) Guo, X.; Puniredd, S. R.; Baumgarten, M.; Pisula, W.; Müllen, K. *Adv. Mater.* **2013**, *25*, 5467–5472.
- (25) Joshi, S.; Pingel, P.; Grigorian, S.; Panzner, T.; Pietsch, U.; Neher, D.; Forster, M.; Scherf, U. *Macromolecules* **2009**, *42*, 4651–4660.
- (26) Kline, R. J.; McGehee, M. D.; Kadnikova, E. N.; Liu, J.; Fréchet, J. M. J.; Toney, M. F. *Macromolecules* **2005**, *38*, 3312–3319.
- (27) Rivnay, J.; Steyrleuthner, R.; Jimison, L. H.; Casadei, A.; Chen, Z.; Toney, M. F.; Facchetti, A.; Neher, D.; Salleo, A. *Macromolecules* **2011**, *44*, 5246–5255.
- (28) Sirringhaus, H.; Brown, P. J.; Friend, R. H.; Nielsen, M. M.; Bechgaard, K.; Langeveld-Voss, B. M. W.; Spiering, A. J. H.; Janssen, R. A. J.; Meijer, E. W.; Herwig, P.; de Leeuw, D. M. *Nature* **1999**, *401* (6754), 685–688.
- (29) Chen, M. S.; Lee, O. P.; Niskala, J. R.; Yiu, A. T.; Tassone, C. J.; Schmidt, K.; Beaujuge, P. M.; Onishi, S. S.; Toney, M. F.; Zettl, A.; Fréchet, J. M. J. *J. Am. Chem. Soc.* **2013**, *135*, 19229–19236.
- (30) Osaka, I.; Saito, M.; Mori, H.; Koganezawa, T.; Takimiya, K. *Adv. Mater.* **2012**, *24*, 425–430.
- (31) Shao, M.; Keum, J.; Chen, J.; He, Y.; Chen, W.; Browning, J. F.; Jakowski, J.; Sumpter, B. G.; Ivanov, I. N.; Ma, Y.-Z.; Rouleau, C. M.; Smith, S. C.; Geohegan, D. B.; Hong, K.; Xiao, K. *Nat. Commun.* **2014**, *5*, 1–11.
- (32) Verploegen, E.; Mondal, R.; Bettinger, C. J.; Sok, S.; Toney, M. F.; Bao, Z. *Adv. Funct. Mater.* **2010**, *20*, 3519–3529.